Nanotechnology **20** (2009) 305304 (6pp) doi:10.1088/0957-4484/20/30/305304

Transition flow through an ultra-thin nanosieve

S Unnikrishnan[1], H V Jansen[1], F H Falke[1], N R Tas[1], H A G M Van Wolferen[1], M J De Boer[1], R G P Sanders[1] and M C Elwenspoek[1,2]

[1] Transducers Science and Technology Group, MESA+ Institute for Nanotechnology, University of Twente, PO Box 217, 7500 AE Enschede, The Netherlands
[2] FRIAS, University of Freiburg, Albertstrasse 19, D-79194 Freiburg, Germany

E-mail: s.unnikrishnan@ewi.utwente.nl

Received 27 April 2009, in final form 3 June 2009
Published 7 July 2009
Online at stacks.iop.org/Nano/20/305304

Abstract
The fabrication and gas flow characterization of an ultra-thin inorganic nanosieve structured by interference lithography and a bond-micromachining approach are reported. The nanosieve has been observed to exhibit transition gas flow behaviour around atmospheric pressure and ambient temperature. The small lip thickness (45 nm) of the nanopores with respect to their diameter (120 nm) helps in understanding pure transition flow by minimizing interactions between the molecule and inner pore wall. Due to the absence of these collisions, the transition flux is the superimposition of viscous and molecular fluxes without the need for higher-order slip correction. The nanosieve shows a flow selectivity of 3.1 between helium and argon at 20 mbar.

(Some figures in this article are in colour only in the electronic version)

1. Introduction

Inorganic nanoporous membranes have been an intensively studied topic for the past few years with wide applications in the filtration and separation sectors [1, 2]. The usual kind of inorganic nanoporous membranes are randomly porous structures having many tortuous as well as dead-end pores and with a broad pore size distribution. A new class of these membranes—the nanosieves—has lately gained considerable attention with their uniform array of non-tortuous cylindrical pores having superior advantages like narrow pore size distribution and high flux [3–7]. Nanosieves can be classified into one-dimensional (1D) and two-dimensional (2D) morphologies as shown in figure 1. While a 1D nanosieve is defined here as a membrane with pore diameters of around or below a hundred nanometres, a 2D nanosieve additionally has its thickness equal to or less than the size of its nanopores.

There have been a few reports in the literature about 1D nanosieve fabrication and flow characterization [3–5]. Their main disadvantage is that, due to the high aspect ratio of their pores, the transfer pressure drop is quite high. To reduce the flow resistance while hardly affecting the selectivity between species to be separated, the nanosieve needs to be thinned down, thus converting it to a 2D nanosieve. Although there is some literature available on the fabrication of the more fragile 2D nanosieves for fluid filtration and separation applications [6, 7], there has not been much research effort in the direction of understanding their gas flow behaviour, especially in the transition regime.

In this paper, we report the fabrication of an ultra-thin inorganic 2D nanosieve membrane and its characterization with respect to transition flow. The ultra-thin supported nanosieve is realized by wafer scale interference lithography and a bond-micromachining technique and is of 45 nm thickness having clearly defined circular pores of ⌀120 nm. The characteristics of the nanosieve are determined by measuring the flux and selectivity of different gas species at varying mean and differential pressures. The experimental investigations are supported by theoretical formulations derived and adapted from earlier works including that of Graham [8], Sampson [9], Knudsen [10], Dushmann [11] and Clausing [12]. The small lip thickness of its nanopores enables us to understand the pure transition flow through the 2D nanosieve by minimal wall interaction effects [13]. In this work we show that, with an extremely thin membrane and with a well-defined uniform pore structure, the transition flux is the linear addition of the viscous and molecular fluxes without using any fitting parameters. The outline of

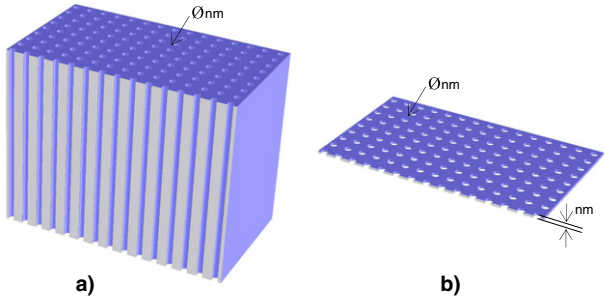

Figure 1. Cross-sectional models of (a) one-dimensional (1D) nanosieve with pore size in nanometres and (b) two-dimensional (2D) nanosieve with pore size and thickness in nanometres.

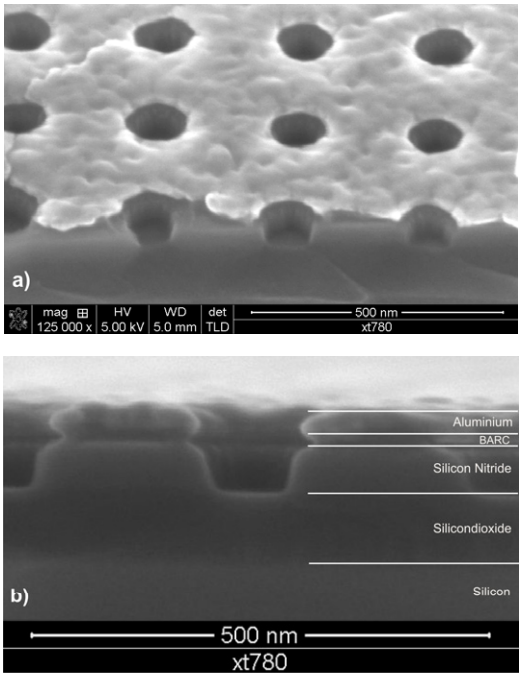

Figure 2. (a) High resolution SEM photograph showing the nanopores etched into the silicon nitride layer with the aluminium mask still on top. (b) Cross section of a pore in silicon nitride also depicting the various other layers.

this paper is as follows. After explaining the fabrication process for the nanosieve membrane, its assembly onto a robust microsieve support is described. Next, the theoretical model and important parameters to estimate the flow through the microsieve supported nanosieve are explained. Finally, discussions on the comparison of estimated flow rates with the measured values are presented.

Being a strong and inert inorganic membrane material, silicon nitride is chosen as the nanosieve material in this work. Laser interference lithography (LIL) [14] is used as the technique to create the pore pattern in the silicon nitride layer. LIL has been shown to be a suitable technique to create sieve patterns by prior research in our group [15, 16]. In this paper, this technique is extended to make large-area thin-film pore patterns and transform them into a supported ultra-thin 2D nanosieve membrane to study gas dynamics through them.

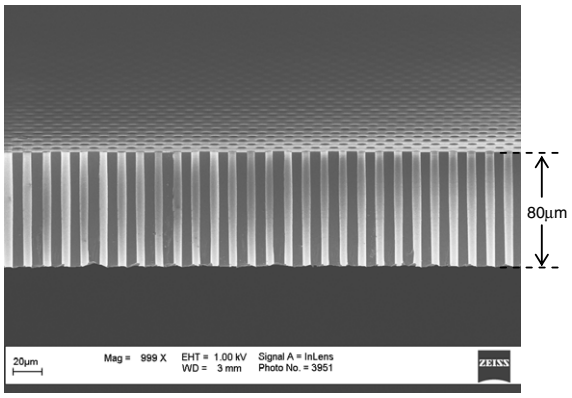

Figure 3. Cross section of the plasma-etched microsieve support showing the straight and parallel micropores of $\varnothing 6\ \mu$m.

2. Fabrication

The fabrication process starts with LPCVD deposition of a 45 nm thick silicon nitride layer on a thermally oxidized silicon carrier wafer. This wafer is then spin-coated with a 20 nm thick bottom anti-reflection coating: BARC layer (DUV 46, Brewer Science Inc.) followed by a 130 nm thick positive photoresist (PEK 500, Sumitomo Chemical Co. Ltd). Using LIL, double exposure of the photoresist at a half-angle of 30° and an exposure dose of 1.1 mJ cm^{-2} are done to generate a square array of posts after development. The pattern reversal is done by a lift-off process in which, after depositing a 20 nm layer of aluminium, the post pattern is inverted to a pore pattern by dissolving the photoresist in acetone. An evaporation process is chosen so that aluminium is directionally deposited over the post pattern, resulting in a shadowing effect which benefits the lift-off procedure. The pattern is then transferred into the underlying BARC and silicon nitride layers via plasma etching, stopping selectively on the 80 nm thick silicon oxide layer underneath (figure 2). The BARC layer is etched with low power (5 W) oxygen plasma under 20 sccm O_2 flow and 10 mTorr chamber pressure, whereas the silicon nitride layer is directionally etched using a 25 W mixed gas plasma of trifluoro-methane (CHF_3) and oxygen flowed at 20 sccm and 5 sccm, respectively, under 10 mTorr chamber pressure. After the creation of the pattern, the next step is to release it by a bond-micromachining approach involving a thin-film transfer technique as explained below. After stripping off the aluminium mask and the BARC layer, the nanopatterned carrier wafer is thoroughly cleaned and fusion-bonded to a wafer having a silicon microsieve structure. The silicon microsieve has well-defined straight pores of $\varnothing 6\ \mu$m (figure 3) and is created by a deep reactive ion etching (DRIE) process using a time-multiplexed Bosch recipe, where sulfur hexafluoride (SF_6) and trifluoro-methane (CHF_3) are used as the etching gas and passivating gas, respectively [17]. This microsieve wafer acts as a robust supporting structure to the nanosieve membrane after it is released by etching away the carrier wafer [18]. The silicon oxide membrane acts as a stop layer during the carrier wafer etching step, thus protecting the silicon nitride nanosieve from damage. Subsequently,

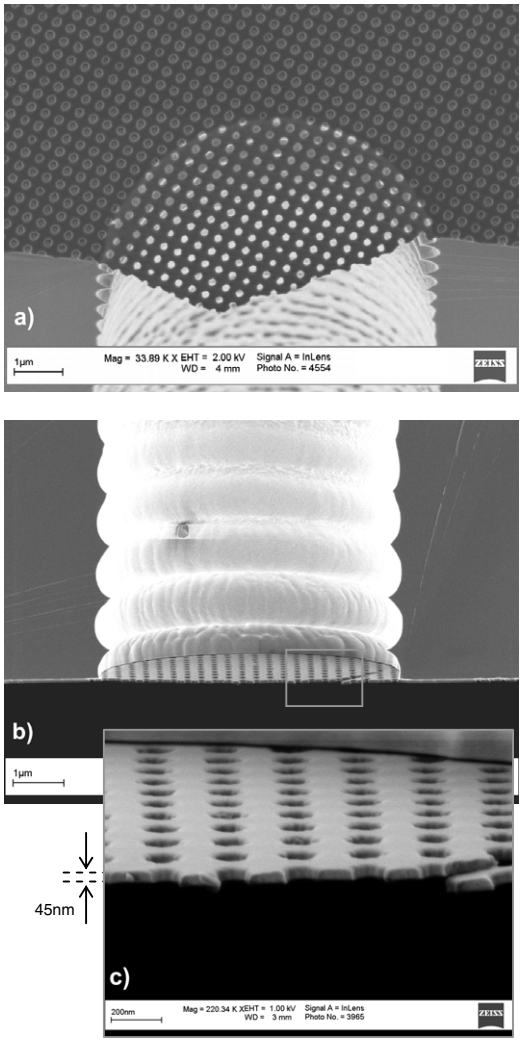

Figure 4. The released nanosieve membrane bonded on the microsieve support etched using the DRIE process. (a) View from the top of the nanosieve membrane, (b) view from inside a micropore, (c) zoomed view of the free-hanging nanosieve.

this protecting oxide is selectively removed in 1%HF solution to finally release the 2D nanosieve. Figure 4 shows the SEM images of the nanosieve suspended on a micropore of the support. Across the wafer, the LIL exposure exhibits pore size non-uniformity due to the Gaussian intensity profile of the laser beam. This intensity variation was found to be causing a 10% standard deviation in the feature sizes measured within an area of 50 mm × 50 mm at the middle of the wafer.

The nanopores for the samples chosen for our experiments are of 120±10 nm in diameter, resulting in a porosity of ∼18%. Together with the microsieve, which has a porosity of 18%, the final void fraction of the total sieve (nanosieve supported on microsieve) is about 3.2%.

In order to test gas flow behaviour through it, the total sieve is fusion-bonded at 800 °C onto 6 mm long Duran® glass tubes of ⌀3 mm inner diameter (see figure 5), which can be sealed within standard Swagelok® connectors [19].

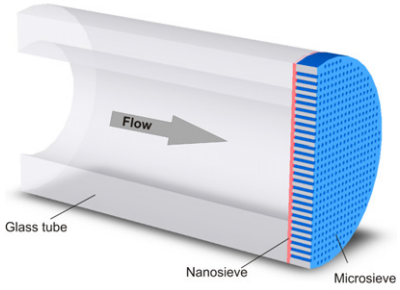

Figure 5. Cross-sectional illustration of the microsieve supported nanosieve fusion-bonded on a glass tube.

3. Theory and characterization

Gases behave as a continuum with viscous effects dominating when the size of the pore through which it flows is significantly larger than the mean free path of the gas (i.e. $d \gg \lambda$). As the pore diameter is reduced to a size much smaller than the mean free path of the gas (i.e. $d \ll \lambda$), it starts to act molecularly, i.e. as a collection of molecules moving independently through largely empty space. When the pore diameter is of the same order of magnitude as the mean free path of the gas (i.e. $d \approx \lambda$), the flow behaviour is termed to be in transition between viscous and molecular flows, which is the case for the pores of the 2D nanosieve around atmospheric pressure. Initial efforts to quantify transition flow were made by Knudsen [10] by means of studying flow through capillaries. His studies led to the dimensionless number known as the Knudsen number: $K_n = \lambda/d$. Based on the Knudsen number, the flow behaviour of gases can be categorized into viscous ($K_n < 0.01$), transition ($0.01 < K_n < 1$) and molecular ($K_n > 1$) flow regimes [11]. Although Knudsen had tried to approximate the transition flow through capillaries as a superimposition of viscous and molecular fluxes, he had to include correction terms to account for wall interaction effects. Moreover, intermolecular collisions will limit the molecular transport drastically when the length of the capillary is well above the mean free path of the gas. These effects become less significant and the flux superimposition technique could work when the length of the capillary is reduced below the mean free path of the gas, as proven by Lund and Berman [20] while doing experiments with tubes of different aspect ratios. Later on, Eickmann and Werner [21] showed the applicability of the superimposition technique for approximating flow through porous membranes. However, due to the ambiguously defined pore size and shape of their considerably thicker membranes, membrane-morphology-dependent correction factors had to be used as fitting parameters. In this work we show that, when the membranes are made extremely thin and with well-defined pores, the transition flux is indeed the linear addition of the viscous and molecular fluxes, without the need of any fitting parameters.

For an easy understanding of the flow through the total sieve, an equivalent circuit model is developed using an electrical analogy as shown in figure 6. The equivalent circuit

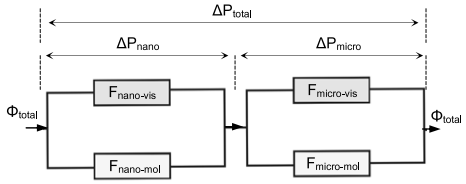

Figure 6. Equivalent circuit model for the mass flows through the microsieve and nanosieve. ΔP, Φ and F stand for pressure drop, mass flow and flow conductance, respectively.

model is based on the following equations:

$$\Delta P_{\text{total}} = \Delta P_{\text{micro}} + \Delta P_{\text{nano}} \tag{1}$$

$$\Phi_{\text{total}} = \Phi_{\text{micro}} = \Phi_{\text{nano}} \tag{2}$$

where ΔP and Φ stand for pressure drop (Pa) and mass flow (mol s^{-1}), respectively. The subscripts micro and nano relates the aforementioned variables respectively to the microsieve and nanosieve. Equation (2) is valid only in the case of fluxes being expressed as mass flows (for example, in unit sccm, i.e. cm^3 min^{-1} at STP) due to the conservation of mass for the gas while passing through the membrane. Following the attempts of Knudsen [10], we quantify the theoretical transition flux as a linear addition of the viscous and molecular fluxes:

$$\Phi_{\text{micro}} = \Delta P_{\text{micro}}(F_{\text{micro-vis}} + F_{\text{micro-mol}}) \tag{3}$$

$$\Phi_{\text{nano}} = \Delta P_{\text{nano}}(F_{\text{nano-vis}} + F_{\text{nano-mol}}) \tag{4}$$

where F represents the flow conductance (mol s^{-1} Pa^{-1}) through the sieves and the subscripts vis and mol indicate viscous and molecular flows, respectively, corresponding to the microsieve and nanosieve. The physical background of this superimposition is that the total flux is a summation of the collective drift of the gas molecules (i.e. viscous flux) and a flow due to statistical imbalance of the thermal molecular motion (i.e. molecular flux) caused by an applied pressure difference across the sieves. Flow conductance for both the sieves in the molecular flow regime are as follows [8, 10–12, 22]:

$$F_{\text{micro-mol}} = \frac{A\kappa_{\text{micro}}}{\sqrt{2\pi MRT}}\left(1 + \frac{3t_{\text{micro}}}{8r_{\text{micro}}}\right)^{-1} \tag{5}$$

$$F_{\text{nano-mol}} = \frac{A\kappa}{\sqrt{2\pi MRT}}\left(1 + \frac{t_{\text{nano}}}{2r_{\text{nano}}}\right)^{-1} \tag{6}$$

where M is the molar mass (kg mol^{-1}) of the gas used, R is the universal gas constant (J mol^{-1} K^{-1}), T is the ambient temperature (K), A is the area of the free-hanging sieve bonded on the glass tube (m^2), κ is the net porosity of the total sieve (which is a product of the porosity of the nanosieve κ_{nano} and the porosity of the microsieve κ_{micro}), r_{micro} and r_{nano} are the radii (m) of the micropore and nanopore, respectively, and t_{micro} and t_{nano} are the respective thicknesses (m) of the microsieve and nanosieve. The terms $(1+3t/8r)$ and $(1+t/2r)$ are the Clausing factors of the microsieve with long pores and nanosieve with short pores, respectively. The flow conductance for the viscous regime can be written as [9, 23, 24]

$$F_{\text{micro-vis}} = \frac{A\kappa_{\text{micro}} r_{\text{micro}} P_{\text{micro}}}{3\eta RT\pi}\left(1 + \frac{8t_{\text{micro}}}{3\pi r_{\text{micro}}}\right)^{-1} \times (1 - f(\kappa_{\text{micro}}))^{-1} \tag{7}$$

$$F_{\text{nano-vis}} = \frac{A\kappa r_{\text{nano}} P_{\text{nano}}}{3\eta RT\pi}\left(1 + \frac{8t_{\text{nano}}}{3\pi r_{\text{nano}}}\right)^{-1}(1 - f(\kappa_{\text{nano}}))^{-1}. \tag{8}$$

Here, P_{micro} and P_{nano} are the respective arithmetic mean pressures (Pa) in the microsieve and nanosieve and η is the viscosity (Pa s) of the gas used. The term $(1 + 8t/3\pi r)$ describes the frictional losses experienced by the gas due to interaction with the pore surface and $(1 - f(\kappa))$ quantifies the influence of flow through the neighbouring pores on the flow through a single pore. In order to account for compressibility effects of gas flow, Sampson's viscous orifice flow expression [9] is modified using the ideal gas law. Substituting the flow conductances in equations (3) or (4), the mass flows through the sieves are determined. The parameter values used in the calculations are listed in table 1. The mass flows are converted from (mol s^{-1}) to (sccm) (1 mol s^{-1} $\approx$ 1.344×10^6 sccm).

The schematic of the gas flow set-up used for characterization is illustrated in figure 7. Initial experiments are performed by flowing air at 296 K, at varying mean pressures (from above-atmospheric down to sub-atmospheric pressures of ~0.02 bar) and at fixed differential pressure across the total sieve. For measurement at above-atmospheric pressures, after setting the inlet pressure at the desired value and fully opening flow regulator 1, flow regulator 2 is adjusted till the desired pressure drop is shown by the differential pressure sensor. Any change in the inlet pressure is corrected again with the pressure regulator. For sub-atmospheric

Table 1. Parametric values used for calculating flow conductances.

Parameters	Values
Ambient temperature, T	296 K
Active area of total sieve, A	7.548×10^{-6} m^2
Porosity of the microsieve, κ_{micro}	18.1%
Porosity of the nanosieve, κ_{nano}	17.3%
Radius of the micropore, r_{micro}	3×10^{-6} m
Radius of the nanopore, r_{nano}	62.5×10^{-9} m
Thickness of the microsieve, t_{micro}	80×10^{-6} m
Thickness of the nanosieve, t_{nano}	45×10^{-9} m
Correction microsieve $(1 - f(\kappa_{\text{micro}}))$	0.9726
Correction nanosieve $(1 - f(\kappa_{\text{nano}}))$	0.9743
Viscosity, η at 296 K	Hydrogen: 8.86×10^{-6} Pa s Helium: 1.97×10^{-5} Pa s Nitrogen: 1.78×10^{-5} Pa s Air: 1.84×10^{-5} Pa s Argon: 2.26×10^{-5} Pa s
Molecular mass, M	Hydrogen: 0.002 02 kg mol^{-1} Helium: 0.004 003 kg mol^{-1} Nitrogen: 0.028 01 kg mol^{-1} Air: 0.028 97 kg mol^{-1} Argon: 0.039 95 kg mol^{-1}

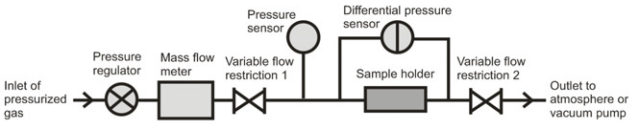

Figure 7. Schematic representation of the gas flow set-up.

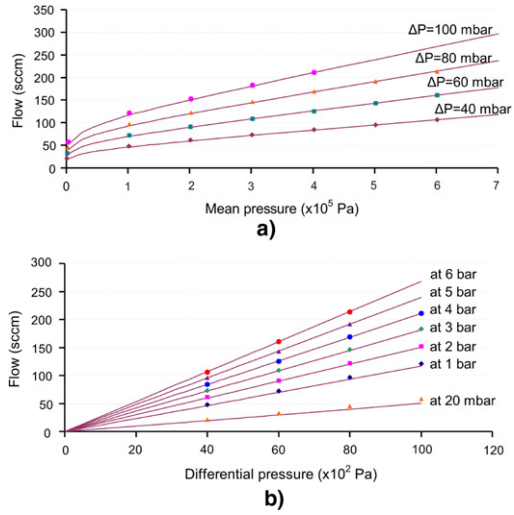

Figure 8. Air fluxes through the nanosieve (a) for varying mean pressures recorded at different differential pressures and (b) for varying differential pressures recorded at different mean pressures. The solid lines represent the theoretical estimate for the flows. The flow measurement errors range from ±1% for low flows to ±0.6% for high flows. The pressure measurement error lies within a margin of ±2% for around atmospheric pressure and gets smaller for higher pressures. The error in the differential pressure is negligibly small.

measurements, the inlet pressure is set to 1 bar and flow regulator 2 is left fully open. Then, the pressure drop across the sieve is tuned solely using flow regulator 1. The outlet of the set-up is connected to a vacuum pump in the latter case unlike in the former case where it is open to the atmosphere. The sensors used in the gas flow set-up have the following error margins: the differential pressure sensor (Sensortechnics GmbH) has an error margin of 0.2% on full scale 0.344 bar. The pressure sensor (Sensortechnics GmbH) has an error margin of 0.5% on full scale 5 bar and registers the pressure above 1 atmosphere. The mass flow through the nanosieve is registered by a mass-flow meter (Bronkhorst High-Tech b.v.) having an error margin of 0.5% on readout and 0.1% on full scale 240 sccm or mln min^{-1}.

4. Results and discussion

Plotted in figure 8(a) are the measurement points and theoretical curves of air flows through the sieve, which show a good match between the model and experiments. An average pore size of ⌀125 nm is assumed for the theoretical calculations, which is within the size measurement error limits. At higher mean pressures, a linear increasing trend can be observed in the measured flow, which is an effect of the viscous flow behaviour. At atmospheric pressure and 100 mbar

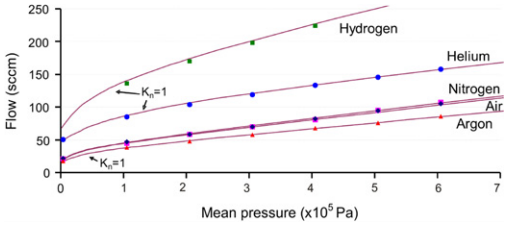

Figure 9. Fluxes of different gases at varying mean pressures measured at a fixed differential pressure of 40 mbar. The solid lines represent the theoretical estimate for the flows.

trans-membrane pressure, the air flux through the tube bonded sieve is 7.56 l h^{-1} (i.e. 121 sccm), which is equivalent to 10.7×10^6 l h^{-1} m^{-2} bar^{-1}.

At sub-atmospheric pressures, the flow lines are not linear, because at low mean pressures—dictated by the free molecular flux—the Clausing loss of the microsieve becomes significant. As estimated, the flow at lower mean pressures does not reach zero, but a value equal to the molecular flux through the sieve. The measurements can be viewed differently by plotting the total mass flow against varying differential pressures across the sieve as shown in figure 8(b). The curves here being linear proves that the kinetic losses of the sieve are negligible.

Since the total flow has a considerable contribution from the molecular flow, the nanosieve should show some selectivity between gas molecules based on the difference in their molecular mobilities. The maximum selectivity between two gases in the molecular flow regime is the square root of the ratio of their molecular masses [8]. Shown in figure 9 are results of experiments performed with gases of different molecular weights, which reveal a definite mass-based selectivity (for large K_n values). The selectivities are determined with pure gas flow experiments. It can be observed in this graph that helium starts to enter the molecular regime at a higher pressure than the others. This is because of its longer mean free path compared to the other gases at the same pressure. The flows of nitrogen and air are overlapping due to their similar molecular weights. Argon, the heaviest of the lot, has the lowest flux.

The He/Ar selectivity is 3.1 at 20 mbar mean pressure, which is quite in accordance with the theoretical expectation. The selectivity could be made even better by eliminating the viscous effects of the flow by reducing further the pore sizes. With LIL technology, it is possible to achieve nanopatterns down to around 60 nm in dimension [16]. Or, alternatively, the pore size of the current nanosieves can be reduced by depositing an extra silicon nitride layer on it using the chemical vapour deposition technique [7]. The selectivity could also be improved by placing multiple sieves in a cross-flow configuration. A selectivity of 2.32 is observed around 1 bar mean pressure due to the difference in viscosity of the gases. This viscosity-based selectivity at higher pressures would vanish when mixed gas experiments are performed.

The strength of the total sieve bonded on the glass tube of ⌀3 mm inner diameter was found to be at least 5 bar of trans-membrane pressure, measured to the limit of our pressure sensors. The sieve assembled onto the glass tube was tested for mechanical integrity up to 700 °C.

5. Conclusion

To summarize, a nanosieve with 45 nm thickness and 120 nm pore diameter has been fabricated using nanomachining techniques. The ultra-thin nanosieve is supported on a robust microsieve having $\varnothing 6$ μm pores and 80 μm thickness via a bond-micromachining technique. The composite sieve structure has been characterized to understand the flow behaviour of different gases at varying mean pressures and trans-membrane pressures. A mass-flow-based model has been developed using an electrical analogy to determine the total flux through the composite sieve. The transition flow regime has been the focus of the study, where the flux through the 2D nanosieve is shown to be a linear addition of viscous and molecular fluxes, without using any fitting parameters. The extremely small lip thickness of the nanopores enabled the quantification of pure transition flow by minimizing the pore wall interaction effects of the gas molecules. A major contribution to the net flux from molecular flow was observed for the nanosieve at atmospheric pressure. The nanosieve clearly demonstrates a molecular-mass-based selectivity between different gas species. Due to its geometrically regular nanopore pattern and small thickness, the 2D nanosieve can deliver higher fluxes at low pressure drops, which makes it attractive for various applications including particle filtration, air sterilization or gas separation.

Acknowledgments

The authors would like to thank Dutch Technology Foundation STW for funding this project. Special thanks are due to Johnny Sanderink and Mark Smithers for the High Resolution SEM pictures. Thanks are also due to Rob Lammertink for useful discussions.

References

[1] Tsuru T 2001 *Sep. Purif. Rev.* **30** 191
[2] De Vos R M and Verweij H 1998 *Science* **279** 1710
[3] Holt J K, Park H G, Wang Y, Stadermann M, Artyukhin A B, Grigoropoulos C P, Noy A and Bakajin O 2006 *Science* **312** 1034
[4] Thormann A, Teuscher N, Pfannmoeller M, Rothe U and Heilmann A 2007 *Small* **3** 1032
[5] Gruener S and Huber P 2008 *Phys. Rev. Lett.* **100** 064502
[6] Kuiper S, Van Rijn C J M, Nijdam W and Elwenspoek M 1998 *J. Membr. Sci.* **150** 1
[7] Tong H D, Jansen H V, Gadjil V J, Bostan C G, Berenschot E, Van Rijn C J M and Elwenspoek M 2004 *Nano lett.* **4** 283
[8] Graham T 1846 *Phil. Trans. R. Soc.* **136** 573
[9] Sampson R A 1891 *Phil. Trans. R. Soc.* A **182** 449
[10] Knudsen M 1909 *Ann. Phys.* **28** 75
Knudsen M 1995 *J. Membr. Sci.* **100** 23 (Engl. Transl.)
[11] Dushmann S and Lafferty J M 1962 *Scientific Foundations of Vacuum Technique* 2nd edn (New York: Wiley)
[12] Clausing P 1932 *Ann. Phys.* **12** 961
Clausing P 1971 *J. Vac. Sci. Technol.* **8** 636 (Engl. Transl.)
[13] Arkilic E B, Breuer K and Schmidt M A 2001 *J. Fluid Mech.* **437** 29–43
[14] Kapon E and Katzir A 1982 *J. Appl. Phys.* **53** 1387
[15] Van Rijn C J M, Veldhuis G J and Kuiper S 1998 *Nanotechnology* **9** 343
[16] Kuiper S, Van Wolferen H, Van Rijn C J M, Nijdam W, Krijnen G and Elwenspoek M 2001 *J. Micromech. Microeng.* **11** 33
[17] Jansen H, De Boer M, Unnikrishnan S, Louwerse M and Elwenspoek M 2009 *J. Micromech. Microeng.* **19** 033001
[18] Unnikrishnan S, Jansen H, Berenschot E and Elwenspoek M 2008 *J. Micromech. Microeng.* **18** 064005
[19] Unnikrishnan S, Jansen H, Berenschot E, Mogulkoc B and Elwenspoek M 2009 *IEEE Proc. MEMS* p 324
[20] Lund L M and Berman A S 1966 *J. Appl. Phys.* **37** 2489–95
Lund L M and Berman A S 1966 *J. Appl. Phys.* **37** 2496–508
[21] Eickmann U and Werner U 1985 *German Chem. Eng.* **8** 186
[22] Kennard E 1938 *Kinetic Theory of Gases* (New York: McGraw-Hill)
[23] Dagan Z, Weinbaum S and Pfeffer R 1983 *Chem. Eng. Sci.* **38** 583
[24] Tio K and Sadhal S S 1994 *Appl. Sci. Res.* **52** 1